ACS central science

http://pubs.acs.org/journal/acscii

Research Article

Cooperative Self-Assembly Driven by Multiple Noncovalent Interactions: Investigating Molecular Origin and Reassessing Characterization

Samaresh Samanta, Parth Raval, G. N. Manjunatha Reddy,* and Debangshu Chaudhuri*

Cite This: *ACS Cent. Sci.* 2021, 7, 1391−1399

Read Online

ACCESS | Metrics & More | Article Recommendations | Supporting Information

ABSTRACT: Cooperative interactions play a pivotal role in programmable supramolecular assembly. Emerging from a complex interplay of multiple noncovalent interactions, achieving cooperativity has largely relied on empirical knowledge. Its development as a rational design tool in molecular self-assembly requires a detailed characterization of the underlying interactions, which has hitherto been a challenge for assemblies that lack long-range order. We employ extensive one- and two-dimensional magic-angle-spinning (MAS) solid-state NMR spectroscopy to elucidate key structure-directing interactions in cooperatively bound aggregates of a perylene bisimide (PBI) chromophore. Analysis of $^{1}H-^{13}C$ cross-polarization heteronuclear correlation (CP-HETCOR) and $^{1}H-^{1}H$ double-quantum single-quantum (DQ-SQ) correlation spectra allow the identification of through-space $^{1}H\cdots^{13}C$ and $^{1}H\cdots^{1}H$ proximities in the assembled state and reveals the nature of molecular organization in the solid aggregates. Emergence of cooperativity from the synergistic interaction between a stronger π-stacking and a weaker interstack hydrogen-bonding is elucidated. Finally, using a combination of optical absorption, circular dichroism, and high-resolution MAS NMR spectroscopy based titration experiments, we investigate the anomalous solvent-induced disassembly of aggregates. Our results highlight the disparity between two well-established approaches of characterizing cooperativity, using thermal and good solvent-induced disassembly. The anomaly is explained by elucidating the difference between two disassembly pathways.

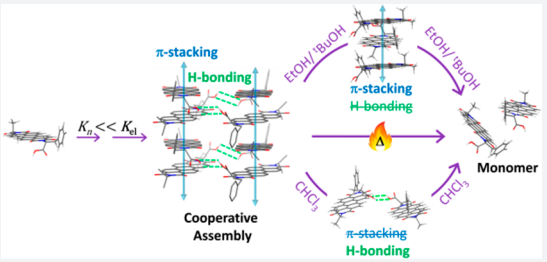

INTRODUCTION

Self-assembled one-dimensional organic nanostructures hold great promise in the area of systems chemistry and material science, and much of the success is owed to recent advances made in the area of programmable supramolecular polymerization.[1,2] By virtue of reversibility and relaxed geometric restrictions, noncovalent interactions can drive a molecular self-assembly through multiple pathways and lead to a variety of assembled structures.[3−6] However, in order to maximize performance, it is critical to achieve the desired assembly with high structural order and narrow polydispersity, while also maintaining a high degree of aggregation. In recent times, programmable supramolecular polymerization strategies have fulfilled this objective using a two-pronged approach: by steering the self-assembly toward a preferred pathway[7−12] and ensuring that the assembled structure grows in a controlled manner.[8−10,13−16] In terms of the underlying mechanism, both pathway selection and controlled growth are achieved through cooperative interactions.[8−14]

In the context of one-dimensional supramolecular polymerization, cooperative growth is characterized by a two-stage process: an initial, less-favored nucleation step that serves as a precursor to more spontaneous growth in the elongation stage. This deferred spontaneity, which results in the appearance of the well-known lag-phase in growth kinetics,[8,14,17] is a consequence of additional noncovalent interactions that come into play after a well-defined nucleus is formed in solution.[18−20] From a molecular design point of view, encoding such precise control over the sequence and chronology of noncovalent interactions is nontrivial. While empirical observations suggest a correlation between multiple noncovalent interactions and cooperativity,[8−15,20−25] there are notable exceptions too.[6,23,26] This underscores the need for a molecular-level characterization of noncovalent interactions that could elucidate how different interactions influence each other nonadditively and could lead to the development of a rational design principle to achieve cooperativity. Crystal structure can provide valuable information about the nature of molecular packing and the interactions involved, but its applicability is severely limited in most supramolecular assemblies that are inherently inhomogeneous, and/or lack long-range structural ordering. Small angle X-ray and/or neutron scattering techniques can look into the morphological

Received: May 19, 2021
Published: July 22, 2021

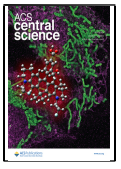

heterogeneities of a molecular assembly but cannot comment on the nature of noncovalent interactions.[27] Only in a few instances of hydrogen-bonded self-assemblies, a rationalization of cooperativity in terms of its molecular origin was done retrospectively, with the aid of computational methods and explicit calculation of stabilization energy per monomer.[28−30]

While investigating the molecular origin of cooperativity is challenging, its characterization and quantification are considered relatively straightforward. This typically involves monitoring the growth of a molecular self-assembly in solution, expressed in terms of the fraction of aggregated species or normalized degree of aggregation (α_{Agg}), as a function of either solution temperature,[31,32] monomer concentration,[33] or solvent composition.[34] Relevant thermodynamic parameters are extracted by analyzing these plots using appropriate mathematical models. All three approaches mentioned above, namely temperature, concentration, and solvent-composition dependence of α_{Agg}, are considered equivalent in terms of the thermodynamic quantities one can obtain about the growth process. Therefore, preferring one approach over the other depends on the system under study, primarily governed by whether a particular variable can be suitably tuned to access the entire self-assembly equilibrium, from monomer ($\alpha_{Agg} = 0$) to the fully aggregated state ($\alpha_{Agg} = 1$).

The present work addresses both aspects of cooperativity discussed above. We employ an extensive magic-angle-spinning (MAS) solid-state NMR spectroscopy approach to investigate the origin of cooperativity in molecular self-assembly. MAS NMR does not require long-range structural order, allowing characterization of the local structure and dynamics of supramolecular assemblies.[35−38] Notably, solid-state NMR spectroscopy has been previously used to investigate local ordering in disordered aggregates of molecular dyes.[39] Further, one (1D) and two-dimensional (2D) MAS NMR techniques have been employed to understand key structure-directing interactions and phase behaviors in molecular self-assembly.[40−45] With regards to the characterization of cooperative self-assembly, we show that the presumed equivalence of different experimental approaches is not strictly valid, thus highlighting the need to exercise caution in the analysis of solvent-composition dependent degree of aggregation, α_{Agg}.

RESULTS AND DISCUSSION

Cooperativity: Quantification and Molecular Origin. Figure 1a presents **PBI-1**, an unsymmetrically substituted perylene bisimide (PBI) with two prominent noncovalent interaction motifs: the aromatic PBI chromophore with strong π-stacking[46] ability and the phenylalanine (Phe) side-group capable of hydrogen bonding. In methylcyclohexane (MCH), **PBI-1** spontaneously aggregates with an H-type coupling between the neighboring chromophores. Figure 1b presents the evolution of optical absorption spectra as a solution of **PBI-1** in MCH (15 μM) is heated under thermodynamic control (1 K/min). The room temperature spectrum of H-aggregated **PBI-1** is characterized by an overall lowering of the absorption cross-section and a reduced 0−0 (515 nm) to 0−1 (479 nm) absorbance ratio (A_{0-0}/A_{0-1}) of 1.06. The broad, featureless absorption band in the 550−630 nm range is indicative of a rotationally twisted stacking of PBI chromophores, a feature commonly observed in PBI based H-aggregates.[47] Disassembly at higher temperatures is evident from the overall increase in the absorbance and a monomer-like A_{0-0}/A_{0-1} ratio of 1.52. A concomitant disappearance of

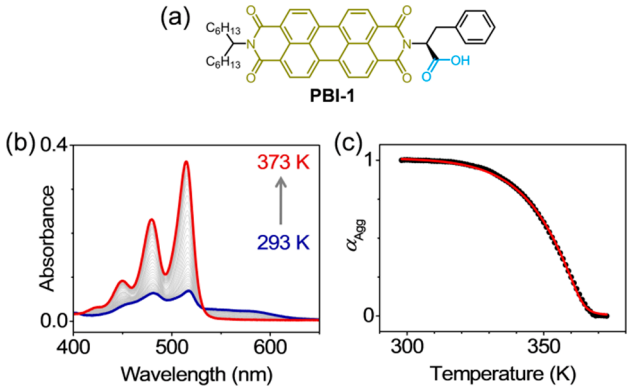

Figure 1. Cooperative self-assembly of **PBI-1**. (a) Molecular structure of **PBI-1**, showing the motifs responsible for π-stacking (olive) and hydrogen-bonding (blue). (b) Temperature-dependent optical absorption spectra of **PBI-1** aggregates in methylcyclohexane (15 μM). (c) Variation of α_{Agg} with temperature, derived from the 0−0 absorbance at 515 nm. The red line shows the simulated curve generated using mass-balance model for $\sigma = 6.3 \times 10^{-4}$, at 293 K.

the low-energy absorption band gives rise to a sharp isosbestic point at 532 nm. α_{Agg} estimated from the absorbance at 515 nm exhibits a distinct nonsigmoidal profile (Figure 1c) that is characteristic of a cooperative self-assembly. Simulating the temperature-dependence of α_{Agg} using the mass-balance model that takes into account an equilibrium between monomeric and aggregated **PBI-1** in solution (Supporting Information, section 3)[31] afforded a very good agreement with the experimental data. Thermodynamic parameters that characterize the nucleation and elongation stages of growth are presented in Table S1 (Supporting Information). The most important takeaway from the analysis of α_{Agg} vs T is σ, the degree of cooperativity, expressed in terms of the ratio of nucleation to elongation stage equilibrium constants ($\sigma = K_n/K_{el}$). A low value of $\sigma = 6.3 \times 10^{-4}$ (at 293 K) translates to a 1600-fold increase in the elongation stage equilibrium constant, thus indicating a high degree of cooperativity in **PBI-1** aggregates. Thermal disassembly of **PBI-1** aggregates was also monitored using CD spectroscopy (Supporting Information, Figure S4a). **PBI-1** aggregates in MCH exhibit a positive bisignated Cotton effect, suggesting a right-handed helical arrangement of PBI chromophores.[48] Analysis of the temperature dependent α_{Agg}, evaluated from the disappearance of CD signal upon heating (Figure S4b), agrees remarkably well with that of absorption spectroscopy: a cooperative assembly with $\sigma = 6.06 \times 10^{-4}$.

In order to gain an insight into the molecular origin of cooperativity and the role of multiple interactions, we carried out a detailed MAS NMR investigation of solid **PBI-1** aggregates grown from MCH solution. Figure 2a presents the ^{1}H MAS NMR spectrum of **PBI-1** aggregates. One can distinguish proton resonances corresponding to different functional groups of **PBI-1** (assignments are color-coded as depicted in schematic structure and further validated by detailed 2D NMR analyses discussed subsequently): a broad signal from the branched aliphatic side-chain protons at 1.5 ppm, two benzylic protons at 3.2 and 4.2 ppm, two ^{1}H−C_α next to the imide N at ∼5.6 ppm, and an intense signal at 7.3 ppm ascribed to the overlapped contributions from phenyl and PBI protons. We focus on the two functional motifs that are primarily responsible for **PBI-1** self-assembly.

https://doi.org/10.1021/acscentsci.1c00604
ACS Cent. Sci. 2021, 7, 1391−1399

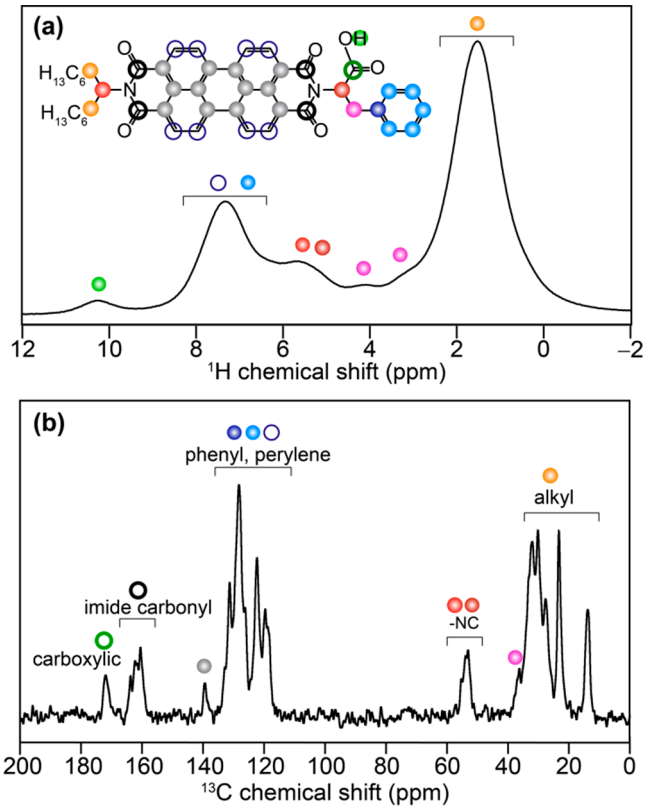

Figure 2. Solid-state 1D NMR spectra of solid **PBI-1** aggregates acquired at 18.8 T (a) ^{1}H MAS NMR (^{1}H Larmor frequency = 800.1 MHz) recorded at 56 kHz MAS and (b) ^{13}C CP-MAS NMR spectrum (^{13}C Larmor frequency = 201.2 MHz) acquired at 50 kHz MAS using 2 ms CP contact time. ^{1}H and ^{13}C signals correspond to aliphatic and aromatic groups are colored as depicted in the inset to (a).

A comparison with the solution state ^{1}H NMR spectrum of molecularly dissolved **PBI-1** in $CDCl_3$ (Supporting Information, Figure S1) reveals that the chemical shift difference ($\Delta\delta$) between phenyl and PBI protons is greatly diminished in solid aggregates. In particular, the large shift toward lower frequency values ($\Delta\delta \sim 1.2$ ppm) experienced by the PBI protons is an indication of strong π-stacking between PBI chromophores.[49−51] Such stacking can expose the protons of one PBI unit to the ring current of the neighboring PBI, resulting in a strong shielding. The spectrum also features a broad signal at 10.2 ppm, arising from weak hydrogen bonding interactions between carboxylic groups. This is corroborated by existing literature on the correlation between −COOH proton chemical shift and the strength of hydrogen-bond for a variety of carboxylic acids.[52] It is possible that a weaker hydrogen-bonding between carboxyl acid side groups synergistically assists a stronger π-stacking interaction between the PBI units to give rise to cooperativity in self-assembled **PBI-1**.[50] In the ^{13}C cross-polarization (CP) MAS NMR spectrum of **PBI-1** aggregates (Figure 2b), one can reliably assign signals corresponding to the terminal methyl (14.6 ppm) and intervening methylene (23.8 ppm) carbons of the alkyl side chain, perylene and phenyl group carbons (119−140 ppm), and the carboxylic acid carbon at 172 ppm. The solution-state ^{13}C NMR spectrum (Supporting Information, Figure S2) agrees well with the ^{13}C signals in the aliphatic and aromatic spectral regions. These ^{13}C spectral assignments were further corroborated by DFT calculated chemical shifts (Supporting Information, Figure S5).

Next, we carried out an investigation into ^{1}H···^{13}C proximities using 2D ^{1}H−^{13}C CP heteronuclear correlation (CP-HETCOR) NMR spectroscopy. Analyses of 2D correlation peaks in HETCOR spectroscopy offer a unique way to identify different packing interactions, as well as reconcile that information with the emergence of cooperativity in molecular assembly. An advantage of 2D ^{1}H−^{13}C HETCOR NMR experiments lies in the resolution enhancement achieved by spreading ^{1}H and ^{13}C signals into two different frequency dimensions. This enables one to resolve correlation peaks associated with molecularly proximate and dipolar-coupled ^{1}H···^{13}C spin pairs with greater confidence. In order to characterize the *intermolecular* interactions responsible for **PBI-1** self-assembly, it is important to first identify correlation signals that originate from the directly bonded C−H pairs and the ones at close *intramolecular* proximity. In doing so, we analyzed and compared the 2D ^{1}H−^{13}C HETCOR spectra acquired at different CP contact times. A preliminary analysis of 1D ^{1}H → ^{13}C CP signal intensity build-up as a function of the CP contact time revealed significant enhancements of ^{13}C signals for a CP contact time of 4 ms and longer (Supporting Information, Figure S6). This was further corroborated by comparing 2D HETCOR spectra acquired with 2, 3, and 4 ms of CP contact time (Supporting Information, Figure S7 and Table S2), whereby the signals associated with short-range (covalently bonded) and long-range (through-space) ^{1}H···^{13}C proximities are distinguished. A detailed analysis of such 2D correlations associated with *inter-* and *intramolecular* interactions is presented in the Supporting Information (Figure S7c, Table S2).

In the ^{1}H−^{13}C HETCOR spectrum acquired with 4 ms of CP contact time (Figure 3a), 2D ^{1}H−^{13}C signals corresponding to the key structure-directing interactions that drive the assembly of **PBI-1** molecules are indicated in solid and dashed ovals. The most notable of all are the 2D correlation signals between benzylic group (magenta) and the branched alkyl chain (orange dots). 1D ^{1}H line-spectrum traced across the ^{13}C dimension for the benzylic carbons at 37.2 ppm shows an intense peak at 1.8 ppm (Figure 3b), confirming dipolar coupling between the two groups. Similarly, ^{1}H line-spectra corresponding to aliphatic C signals at 27.6 and 31.3 ppm also show sizable intensity at 3.2 ppm (benzylic protons). Interestingly, a similar correlation between terminal methyl carbons (14.5 ppm) and benzylic protons (3.2 ppm) is not apparent. Unlike all dipolar ^{1}H···^{13}C correlations discussed so far, these 2D correlation signals cannot result from intramolecular through-space interactions. Since the participating nuclei (benzylic and alkyl groups) are at opposite ends of the **PBI-1** molecule and thus far separated, these 2D correlation signals present the first unambiguous evidence in favor of an antiparallel stacking. Such antiparallel stacking may bring Phe and branched alkyl groups on neighboring **PBI-1** molecules in close proximity and also give rise to additional 2D correlation signals between phenyl ring carbons (blue) and alkyl protons (orange) at 123.4 (^{13}C) and 1.8 ppm (^{1}H). The 2D peak at 128.6 (^{13}C) and 10.3 ppm (^{1}H) is expected to originate from intermolecular close proximity between the carboxylic acid proton and the aromatic ring C of perylene and is consistent with the analogous 2D peak observed between the carboxylic ^{13}C site (172.8 ppm) and perylene protons (7.8 ppm), as

https://doi.org/10.1021/acscentsci.1c00604
ACS Cent. Sci. 2021, 7, 1391−1399

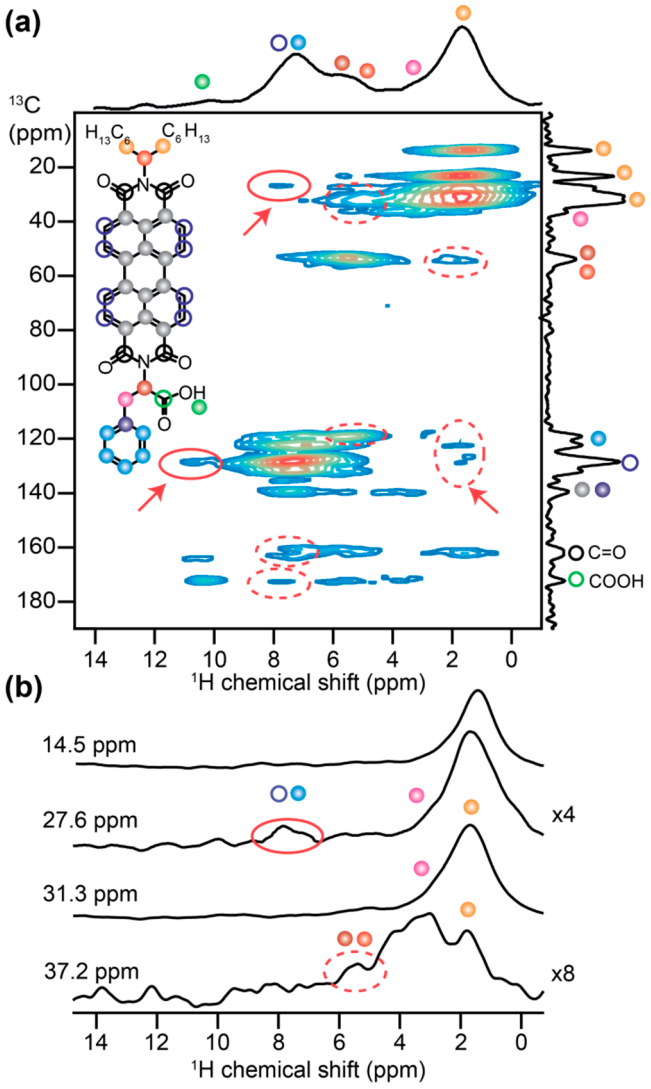

Figure 3. Solid-state (a) 2D ^{1}H−^{13}C HETCOR NMR spectrum of solid **PBI-1** aggregates at 18.8 T, 298 K and 50 kHz MAS using 4 ms CP contact time, and (b) 1D ^{1}H line-spectra traced across the ^{13}C dimension for the aliphatic signals at 14.5, 27.6, 31.3, and 37.2 ppm. Solid and dashed ovals denote the 2D signals originating from purely intermolecular and from a combination of inter- and intramolecular C···H proximities, respectively. ^{1}H and ^{13}C signals associated with aliphatic and aromatic groups are colored as shown in the inset.

depicted in dashed ovals. Such proximity to the aromatic ring can shield the hydrogen-bonded carboxylic acid proton efficiently and be in part responsible for its low chemical shift of 10.3 ppm. In addition to these, 2D peaks involving the ^{13}C signal of C_α (54.4 ppm, burgundy dot) and alkyl side chain protons (1.8 ppm) and between perylene carbons and alkyl protons at 128.6 (^{13}C) and 1.6 ppm (^{1}H) are attributed to intramolecular as well as intermolecular ^{1}H···^{13}C dipole−dipole interactions resulting from the antiparallel stacking of **PBI-1** molecules. In addition, any intermolecular contacts originating from side-on interactions between adjacent π-stacked columns may interfere with the 2D correlation peaks but are likely to be of much weaker intensity. Consequently, disentangling the contribution of ^{1}H−^{13}C dipolar interactions along the π-stacking axis from those originating from side-on interactions is not straightforward.

Information on local ^{1}H···^{1}H proximities at subnanometer (<0.5 nm) distances can be obtained from ^{1}H double-quantum chemical shifts.[40,45] In a 2D ^{1}H double-quantum (DQ) single-quantum (SQ) correlation spectrum (Figure 4), the DQ

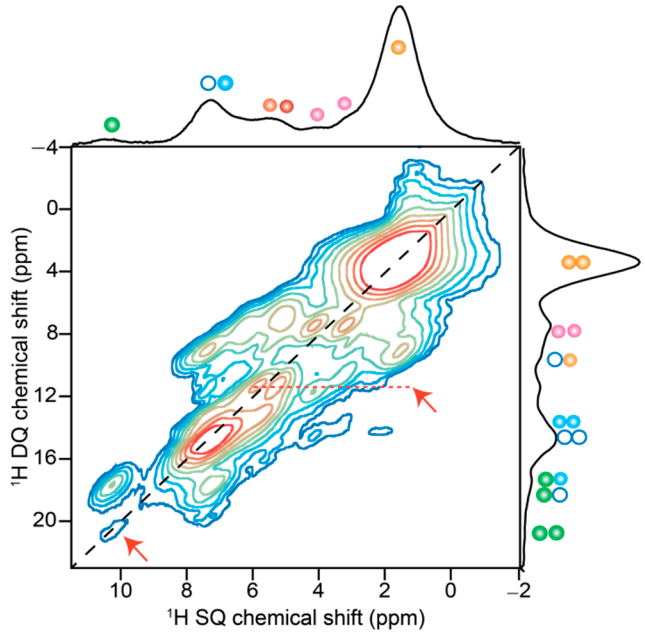

Figure 4. Solid-state 2D ^{1}H−^{1}H DQ-SQ correlation NMR spectrum of solid **PBI-1** aggregates acquired at 800.1 MHz and 56 kHz MAS with 35.6 μs of DQ excitation time. ^{1}H DQ correlation peaks that correspond to inter- and intramolecular H−H proximities (<5 Å) are colored as per the schematic of **PBI-1** in Figures 2 and 3

coherences appear at the sum of two dipole-coupled SQ chemical shifts: the on- and off-diagonal peaks represent chemically equivalent and chemically distinct ^{1}H···^{1}H proximities, respectively. A detailed analysis of 2D correlation intensities arising from *intramolecular* ^{1}H···^{1}H interactions in **PBI-1** aggregates is presented in the Supporting Information (Figure S8, Table S3). Here we focus on the correlations arising out of the *intermolecular* interactions. Notably, the off-diagonal peak at δ_{DQ} of 1.6 + 7.4 = 9.0 ppm suggests through-space proximity between alkyl and aromatic protons, which is also consistent with the appearance of δ_{DQ}, 1.7 + 6.0 = 7.7 ppm and δ_{DQ}, 1.7 + 5.3 = 7.0 ppm peaks that indicate through-space ^{1}H···^{1}H proximities between alkyl protons and ^{1}H−C_α. The latter correlation peaks are better resolved in the ^{1}H DQ spectrum acquired with 71.4 μs DQ excitation time (Supporting Information, Figure S8b and Table S3). Since alkyl and aromatic protons in **PBI-1** are spatially far from each other (>5 Å), a dipolar interaction between them is likely to be intermolecular and is consistent with the antiparallel stacking suggested earlier. Antiparallel stacking of **PBI-1** molecules is best consolidated by the appearance of a reasonably intense ^{1}H DQ coherence at δ_{DQ}, 5.3 + 6.0 = 11.3 ppm (red arrow), which indicates close proximity between two ^{1}H−C_α protons. Clearly, the two ^{1}H−C_α protons of the same **PBI-1** molecule that are at a separation of over 5 Å cannot support such a strong dipolar coupling. A higher intensity of this DQ peak compared to the one at δ_{DQ}= 9.0 ppm suggests that the separation between the pair of ^{1}H−C_α protons across the PBI stack is shorter than that between alkyl and aromatic protons. One expects that to be true for a rotationally twisted stack of **PBI-1** molecules, in

https://doi.org/10.1021/acscentsci.1c00604
ACS Cent. Sci. 2021, 7, 1391−1399

which the separation between the coupled nuclei increases as one moves away from groups that are centrally located, such as $^1H-C_\alpha$, to ones that more peripheral, like alkyl and Phe groups. The ^1H DQ peak at 7.4 + 10.3 = 17.7 ppm presumably arises from a combination of intra- and intermolecular $^1H\cdots{}^1H$ dipolar coupling between carboxylic acid and aromatic protons. Finally, a weak intensity peak at δ_{DQ}, 10.3 + 10.3 = 20.6 ppm (red arrow) indicates hydrogen-bonding between carboxylic acid groups of neighboring **PBI-1** molecules. We bear in mind that an antiparallel stacking of **PBI-1** molecules rules out the possibility of any hydrogen-bonding between −COOH groups along the stacking axis. Therefore, we conclude that the observed hydrogen bonding must be between **PBI-1** molecules belonging to the adjacent stacks. The intensity ratio of DQ peaks at a specific SQ frequency can be used to quantify interatomic distances for isolated $^1H-^1H$ pairs.[53] The intensity ratio of DQ signals at 17.7 and 20.6 ppm at δ_{SQ} = 10.3 ppm is 4:1. From the ratio, we estimate that the distance between carboxylic acid protons of **PBI-1** molecules hydrogen-bonded to each other is about ∼1.26 times greater than the intramolecular $^1H-^1H$ distance between the carboxylic acid proton and the nearest aromatic proton. This once again indicates that the hydrogen bonding interaction in **PBI-1** aggregates is weak. Thus, while π-stacking is largely responsible for the longitudinal growth of **PBI-1** aggregate, a weaker interstack hydrogen-bonding between −COOH groups contributes to its lateral growth. It is conceivable that in the early stages of self-assembly, a stronger π-stacking between **PBI-1** molecules is primarily responsible for molecular association leading to the formation of a nucleus. In the subsequent elongation phase, additional interstack hydrogen-bonding comes into play that complements π-stacking to drive a more spontaneous growth of **PBI-1** aggregates. Overall, the 2D ssNMR experiments provide a rich source of atomic-level information on the cooperatively bound molecular self-assembly, enabled by the identification of key structure directing intermolecular interactions with site-specificity.

Anomalous Solvent-Induced Disassembly. Having elucidated the role of multiple noncovalent interactions in the context of cooperative growth in **PBI-1** aggregates, we investigate the effect of solvent composition on the aggregation process. It is generally accepted that analysis of solvent-composition dependence of α_{Agg} affords very similar information about the self-assembly mechanism as temperature dependence. Analyzing cooperativity from solvent-induced disassembly is therefore a useful alternative for systems, where temperature cannot be suitably varied because of poor solubility and stability issues, or the possibility of a phase-transition.[34] Investigation of solvent-composition dependence involves varying the ratio of a good-to-bad solvent. In our experiments, MCH was used as the bad solvent, whereas the good solvent was chosen by taking into account the specific nature of solvent−**PBI-1** interactions. We carried out two sets of experiments, each with the aim to address a specific noncovalent interaction in **PBI-1** aggregates. Figure 5a presents the effect of *tert*-butanol (^{t}BuOH) on the optical absorption spectra of **PBI-1** aggregates in MCH. Since ^{t}BuOH has strong hydrogen-bonding capabilities, its interaction with the −COOH group disrupts the intermolecular hydrogen bonding between adjacent **PBI-1** molecules causing aggregate disassembly. A plot of α_{Agg} versus the volume fraction of ^{t}BuOH (f), derived from the absorption spectra is presented in Figure 5b. A cursory examination of the plot quite surprisingly

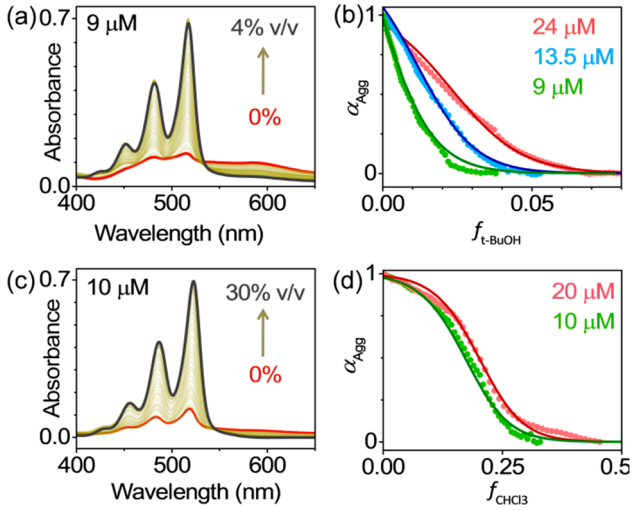

Figure 5. Good solvent induced disassembly. Absorption spectra of **PBI-1** in MCH show progressive disassembly upon increasing the volume fraction of (a) ^{t}BuOH and (c) $CHCl_3$. Analyses of corresponding α_{Agg}vs f plots in b and d show isodesmic behavior. The solid lines are fit to an isodesmic model.

reveals the gradual nature of solvent induced disassembly. Absence of a critical volume fraction across which α_{Agg} changes sharply is not consistent with the notion of a cooperatively bound system. We analyzed the solvent-composition dependence of α_{Agg} within the framework of Goldstein and Stryer's model (Supporting Information, section 8),[33,54] which accounts for monomer association and cooperativity in terms of the elongation stage equilibrium constant (K_{el}) and σ (= K_n/K_{el}), respectively. A key assumption of this model is that the interaction between the aggregate and a good solvent is weak, which allows one to express the free energy change upon monomer binding ($\Delta G^{\circ\prime}$) as a linear function of f:

$$\Delta G^{\circ\prime} = \Delta G^{\circ} + mf$$

Here ΔG° is the free energy change in absence of a good solvent, and m quantifies the denaturing ability of the good solvent. In stark contrast to the temperature-dependence of α_{Agg} presented earlier, the analysis of solvent-composition dependence indicates an isodesmic association in **PBI-1** aggregates (σ = 1), where each monomer association step is equally spontaneous. We reconfirmed this anomalous disassembly behavior by analyzing α_{Agg} vs f_{tBuOH} plots for three different **PBI-1** concentrations (Figure 5b). In each case, the best-fit to the experimental data afforded identical values for the parameters (ΔG°, m), thus validating the robustness of our analyses (see Table S4). In a separate set of experiments, $CHCl_3$ was used as the good solvent to preferentially disrupt π-stacking between **PBI-1** molecules (Figure 5c). Once again, analyses of α_{Agg} vs f_{CHCl3} plots at two different **PBI-1** concentrations (Figure 5d and Table S4) unambiguously suggest isodesmic aggregation. To further support our findings, we carried out solvent-composition dependent CD spectroscopy. Analyses of α_{Agg} vs f obtained from CD spectra reaffirms the agreement with the isodesmic model (Supporting Information, Figure S9). It is worth noting that ΔG° values obtained from the study of solvent-composition dependence are consistently lower (−29 and −36.7 kJ/mol from ^{t}BuOH and $CHCl_3$ induced disassembly, respectively; Table S4) than that obtained from temperature-dependence (−41 kJ/mol,

https://doi.org/10.1021/acscentsci.1c00604
ACS Cent. Sci. 2021, 7, 1391−1399

Table S1) studies. These results clearly stress the need to reassess the applicability of these two approaches in elucidating the self-assembly mechanism.

Deducing the self-assembly mechanism from the disassembly process, be it thermal or solvent-induced, relies on one important assumption: that assembly and disassembly pathways are the same, and one process is just the reverse of the other. We envisage that a departure from this key assumption is responsible for the observed anomaly. One expects the effect of temperature to be straightforward: the monomer association constants (K_{el}, K_n) decrease with increasing temperature, in accordance with the van't Hoff equation. Thus, in the absence of any competing pathways, thermal disassembly follows a course that is same as that of molecular assembly, only in reverse. This reversibility allows one to deduce the self-assembly mechanism from α_{Agg} vs T behavior. The same, however, may not be true for disassembly caused by a good solvent. Since solvent-molecule interactions are very specific in nature, a good solvent can disproportionately affect different noncovalent interactions. Consequently, solvent-induced disassembly can follow a very different trajectory than the self-assembly process. This scenario is especially likely for aggregates, where interactions of very different natures are involved. In order to test this hypothesis, we carried out high-resolution MAS (HR-MAS) NMR titration experiments[55] with variable spinning frequencies using two different good solvents (Figure 6). Our aim was to monitor the evolution of different noncovalent interactions in solid **PBI-1** aggregates at an early stage of solvent-induced disassembly. Figure 6a presents a comparison of ^{1}H HR-MAS NMR spectra of **PBI-1** aggregates in the presence of different weight fractions of ethanol-*d*.[56] A closer examination in the 6−12 ppm range reveals the changes brought about by the good solvent. A gradual loss of signal at 10.3 ppm suggests a progressive weakening of the intermolecular hydrogen-bonding between −COOH groups in the solid aggregate and eventually a complete disruption above 50 wt % of ethanol-*d*. Quite interestingly, the aromatic region of the NMR spectrum shows no change during this titration experiment. Clearly, ethanol causes a selective disruption of hydrogen-bonding, while retaining the π-stacking interactions in solid **PBI-1** aggregates.[57] In contrast, the evolution of ^{1}H MAS NMR spectra upon the addition of $CDCl_3$ to solid **PBI-1** aggregates (Figure 6b) indicates a very different disassembly pathway. Initially, the changes are less distinct, as the spectrum becomes progressively narrower (see Supporting Information). This eventually leads to a significantly well-resolved ^{1}H NMR spectrum at 78 wt % of $CDCl_3$. While the initial line narrowing is presumably due to the breakdown of large aggregates into smaller aggregated domains, a large shift of the aromatic protons to higher frequencies ($\Delta\delta \sim 0.9$ ppm) unambiguously indicates a widespread disruption of PBI π-stacking. A largely unchanged signal at 10.3 ppm corroborates the retention of hydrogen-bonding interaction during titration with $CDCl_3$.

Evidently, the manner in which solvent-induced disassembly is brought about in optical absorption *vis-a-vis* MAS NMR spectroscopy experiments has certain key differences. In the former, shorter soluble aggregates interact with the good-solvent and dissociate in a homogeneous solution-phase process. In contrast, the NMR experiments involved disassembly of much larger aggregates in an inhomogeneous solid-solvent phase. While this prohibits any quantitative comparison of the two disassembly processes, we are able to conclude that a good-solvent induced disassembly is achieved

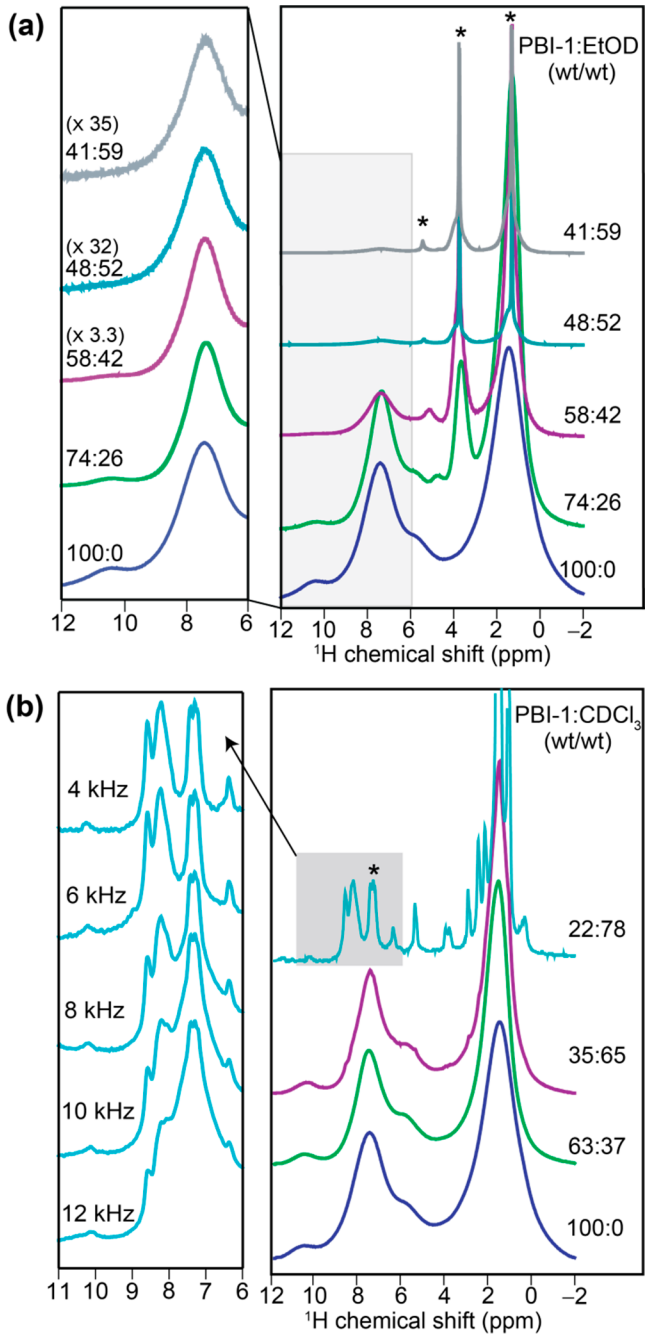

Figure 6. 1D ^{1}H HR-MAS NMR spectra of solid **PBI-1** aggregates acquired at 800.1 MHz as a function of good solvent. (a) Bottom-up stack plot of **PBI-1**:ethanol-*d*, wt/wt, 100:0 (blue), 74:26 (green), 58:42 (violet), 48:52 (cyan), and 41:59 (gray) acquired at 20, 20, 18, 12, and 8 kHz of MAS, respectively. Expanded region (left) depicts normalized intensities of aromatic ^{1}H signals. (b) Bottom-up stack plot of **PBI-1**:$CDCl_3$, wt/wt 100:0 (blue), 63:37 (green), 35:65 (violet) acquired at 20 kHz MAS, and 22:78 (cyan) acquired at 4 kHz MAS. The expanded region (left) depicts aromatic regions of ^{1}H spectra 22:78 (cyan) acquired at different MAS frequencies varying from 4 to 12 kHz (Supporting Information, section 9). * denotes solvent peaks associated with (a) ethanol-*d* (EtOD) and (b) chloroform-*d* ($CDCl_3$).

by disrupting *one-interaction-at-a-time*. Such interaction-specific aggregate dissociation is therefore driven primarily by a lowering of *enthalpic gain* (ΔH_{el}) and is quite distinct from thermal disassembly, which is caused by an increase in the

https://doi.org/10.1021/acscentsci.1c00604
ACS Cent. Sci. 2021, 7, 1391−1399

entropic loss ($-T\Delta S_{el}$). This key distinction between the two disassembly processes can complicate analysis of self-assembly mechanism from the corresponding α_{Agg} plots. We recall that our ability to distinguish between isodesmic and cooperative mechanisms relies on the behavior of α_{Agg} vs f plots in the limit of very low α_{Agg}.[30,34] In this limit, isodesmic aggregates dissociate gradually, whereas cooperatively bound aggregates show a more drastic change in α_{Agg} as the self-assembly process moves from nucleation to elongation regime. It is conceivable that a cooperative aggregate that dissociates *one-interaction-at-a-time* is initially reduced to a weakly bound aggregate state that is held together by a single noncovalent interaction. This change from a multi-interaction to a single-interaction aggregate, though significant from the standpoint of aggregate stability, may not affect the optical absorption spectra, as individual chromophores are still bound together, allowing excitonic interactions to operate. A subsequent disassembly of such monovalent aggregates to free monomers brings the most significant changes in the absorption spectra. Consequently, absorption spectroscopy does not probe the disassembly of the initial cooperatively bound aggregate, but that of an intermediate aggregated state. This intermediate aggregate, which is held together by a single noncovalent interaction, is more likely to exhibit the characteristics of an isodesmic association. Since thermal disassembly is free from such artifacts, temperature dependence of α_{Agg} offers a more reliable method for characterizing self-assembly mechanism in small-molecule aggregates.

CONCLUSIONS

In conclusion, our work addresses two important questions pertaining to cooperative self-assembly of small molecules: molecular origin of cooperative interactions and its characterization. With regards to its origin, a correlation between multiple noncovalent interactions and cooperativity has been empirically observed in the past. However, the basis for such a correlation was not adequately understood in the absence of a detailed characterization of the local structure and the noncovalent interactions stabilizing it, particularly in assemblies that lack long-range order. To this end, we performed solid-state 1D and 2D MAS NMR spectroscopy on cooperatively bound aggregates of **PBI-1**. Our analyses of through-space dipole-coupling between nonbonded $^{1}H\cdots^{13}C$ and $^{1}H\cdots^{1}H$ spin pairs establish that **PBI-1** molecules stack in a rotationally displaced, antiparallel fashion. This dominant π-stacking interaction is complemented by a weaker interstack hydrogen-bonding between the carboxylic acid side groups, resulting in a cooperative self-assembly. The ability to rationalize cooperativity at an atomistic level could offer a way to design molecular building blocks that can be made to assemble along a specific pathway to a desired supramolecular structure. In addition, we compared the conflicting conclusions about the extent of cooperativity in **PBI-1** aggregates, derived from two well-established characterization methods, namely temperature and solvent-composition dependence of α_{Agg}. HR-MAS NMR based titration experiments present a clear evidence that a good-solvent induced disassembly progresses in an interaction-specific manner. In aggregates that employ multiple noncovalent interactions of different kinds, this can lead to an anomalous characterization of cooperativity. Finally, our work underscores the importance of bridging the gap between solution-phase characterization techniques and solid-state structure elucidation using combined solid-state NMR and modeling approaches, the applicability of which extends beyond supramolecular chemistry to other disordered material systems.

ASSOCIATED CONTENT

Supporting Information

The Supporting Information is available free of charge at https://pubs.acs.org/doi/10.1021/acscentsci.1c00604.

Experimental methods, synthesis and characterization, and additional figures and tables (PDF)

AUTHOR INFORMATION

Corresponding Authors

G. N. Manjunatha Reddy − *Univ. Lille, CNRS, Centrale Lille Institut, Univ. Artois, UMR 8181, Unité de Catalyse et Chimie du Solide, F-59000 Lille, France;* orcid.org/0000-0002-8283-2462; Email: gnm.reddy@univ-lille.fr

Debangshu Chaudhuri − *Department of Chemical Sciences, Indian Institute of Science Education and Research (IISER) Kolkata, Mohanpur 741246, India;* orcid.org/0000-0002-8941-4327; Email: dchaudhuri@iiserkol.ac.in

Authors

Samaresh Samanta − *Department of Chemical Sciences, Indian Institute of Science Education and Research (IISER) Kolkata, Mohanpur 741246, India*

Parth Raval − *Univ. Lille, CNRS, Centrale Lille Institut, Univ. Artois, UMR 8181, Unité de Catalyse et Chimie du Solide, F-59000 Lille, France*

Complete contact information is available at: https://pubs.acs.org/10.1021/acscentsci.1c00604

Notes

The authors declare no competing financial interest.

ACKNOWLEDGMENTS

The authors gratefully acknowledge EUSMI (Proposal: E191200366) for access to the 800 MHz solid-state NMR spectrometer. D.C. acknowledges IGSTC (Project: LABEL-ONIK) and IISER Kolkata for financial support. G.N.M.R. acknowledges the University of Lille and region Hauts-de-France for financial support and Prof. Olivier Lafon and Dr. Julien Trébosc for insightful discussions.

REFERENCES

(1) Yin, P.; Choi, H. M. T.; Calvert, C. R.; Pierce, N. A. Programming biomolecular self-assembly pathways. *Nature* **2008**, *451*, 318−322.

(2) Ong, L. L.; Hanikel, N.; Yaghi, O. K.; Grun, C.; Strauss, M. T.; Bron, P.; Lai-Kee-Him, J.; Schueder, F.; Wang, B.; Wang, P.; Kishi, J. Y.; Myhrvold, C.; Zhu, A.; Jungmann, R.; Bellot, G.; Ke, Y.; Yin, P. Programmable self-assembly of three-dimensional nanostructures from 10,000 unique components. *Nature* **2017**, *552*, 72−77.

(3) Lohr, A.; Lysetska, M.; Würthner, F. Supramolecular stereomutation in kinetic and thermodynamic self- assembly of helical merocyanine dye nanorods. *Angew. Chem., Int. Ed.* **2005**, *44*, 5071−5074.

(4) Korevaar, P. A.; George, S. J.; Markvoort, A. J.; Smulders, M. M. J.; Hilbers, P. A. J.; Schenning, A. P. H. J.; De Greef, T. F. A.; Meijer, E. W. Pathway complexity in supramolecular polymerization. *Nature* **2012**, *481*, 492−496.

(5) Fennel, F.; Wolter, S.; Xie, Z.; Plötz, P.-A.; Kühn, O.; Würthner, F.; Lochbrunner, S. Biphasic self- assembly pathways and size-

dependent photophysical properties of perylene bisimide dye aggregates. *J. Am. Chem. Soc.* **2013**, *135*, 18722−18725.
(6) Samanta, S.; Chaudhuri, D. Suppressing excimers in H-aggregates of perylene bisimide folda-dimer: role of dimer conformation and competing assembly pathways. *J. Phys. Chem. Lett.* **2017**, *8*, 3427−3432.
(7) Wagner, W.; Wehner, M.; Stepanenko, V.; Ogi, S.; Würthner, F. Living supramolecular polymerization of a perylene bisimide dye into fluorescent J- aggregates. *Angew. Chem., Int. Ed.* **2017**, *56*, 16008−16012.
(8) Ogi, S.; Sugiyasu, K.; Manna, S.; Samitsu, S.; Takeuchi, M. Living supramolecular polymerization realized through a biomimetic approach. *Nat. Chem.* **2014**, *6*, 188−195.
(9) Ogi, S.; Fukui, T.; Jue, M. L.; Takeuchi, M.; Sugiyasu, K. Kinetic control over pathway complexity in supramolecular polymerization through modulating the energy landscape by rational molecular design. *Angew. Chem., Int. Ed.* **2014**, *53*, 14363−14367.
(10) Greciano, E. E.; Matarranz, B.; Sánchez, L. Pathway complexity versus hierarchical self- assembly in N-annulated perylenes: structural effects in seeded supramolecular polymerization. *Angew. Chem., Int. Ed.* **2018**, *57*, 4697−4701.
(11) Mabesoone, M. F. J.; Markvoort, A. J.; Banno, M.; Yamaguchi, T.; Helmich, F.; Naito, Y.; Yashima, E.; Palmans, A. R. A.; Meijer, E. W. Competing interactions in hierarchical porphyrin self-assembly introduce robustness in pathway complexity. *J. Am. Chem. Soc.* **2018**, *140*, 7810−7819.
(12) Wagner, W.; Wehner, M.; Stepanenko, V.; Würthner, F. Supramolecular block copolymers by seeded living polymerization of perylene bisimides. *J. Am. Chem. Soc.* **2019**, *141*, 12044−12054.
(13) Ogi, S.; Stepanenko, V.; Sugiyasu, K.; Takeuchi, M.; Würthner, F. Mechanism of self-assembly process and seeded supramolecular polymerization of perylene bisimide organogelator. *J. Am. Chem. Soc.* **2015**, *137*, 3300−3307.
(14) Endo, M.; Fukui, T.; Jung, S. H.; Yagai, S.; Takeuchi, M.; Sugiyasu, K. Photoregulated living supramolecular polymerization established by combining energy landscapes of photoisomerization and nucleation−elongation processes. *J. Am. Chem. Soc.* **2016**, *138*, 14347−14353.
(15) Ma, X.; Zhang, Y.; Zhang, Y.; Liu, Y.; Che, Y.; Zhao, J. Fabrication of chiral-selective nanotubular heterojunctions through living supramolecular polymerization. *Angew. Chem., Int. Ed.* **2016**, *55*, 9539−9543.
(16) Kang, J.; Miyajima, D.; Mori, T.; Inoue, Y.; Itoh, Y.; Aida, T. A rational strategy for the realization of chain growth supramolecular polymerization. *Science* **2015**, *347*, 646−651.
(17) Baram, J.; Weissman, H.; Rybtchinski, B. Supramolecular polymer transformation: a kinetic study. *J. Phys. Chem. B* **2014**, *118*, 12068−12073.
(18) De Greef, T. F. A.; Smulders, M. M. J.; Wolffs, M.; Schenning, A. P. H. J.; Sijbesma, R. P.; Meijer, E. W. Supramolecular polymerization. *Chem. Rev.* **2009**, *109*, 5687−5854.
(19) Hunter, C. A.; Anderson, H. L. What is cooperativity? *Angew. Chem., Int. Ed.* **2009**, *48*, 7488−7499.
(20) Mahadevi, A. S.; Sastry, G. N. Cooperativity in noncovalent interactions. *Chem. Rev.* **2016**, *116*, 2775−2825.
(21) Badjic, J. D.; Nelson, A.; Cantrill, S. J.; Turnbull, W. B.; Stoddart, J. F. Multivalency and cooperativity in supramolecular chemistry. *Acc. Chem. Res.* **2005**, *38*, 723−732.
(22) Chung, M.-K.; Lee, S. J.; Waters, M. L.; Gagné, M. R. Self-assembled multi-component catenanes: the effect of multivalency and cooperativity on structure and stability. *J. Am. Chem. Soc.* **2012**, *134*, 11430−11443.
(23) Rest, C.; Kandanelli, R.; Fernandez, G. Strategies to create hierarchical self-assembled structures via cooperative non-covalent interactions. *Chem. Soc. Rev.* **2015**, *44*, 2543−2572.
(24) Kulkarni, C.; Bejagam, K. K.; Senanayak, S. P.; Narayan, K. S.; Balasubramanian, S.; George, S. J. Dipole moment driven cooperative supramolecular polymerization. *J. Am. Chem. Soc.* **2015**, *137*, 3924−3932.
(25) Li, Y.; Wang, Y.; Huang, G.; Gao, J. Cooperativity principles in self-assembled nanomedicine. *Chem. Rev.* **2018**, *118*, 5359−5391.
(26) Kobko, N.; Paraskevas, L.; del Rio, E.; Dannenberg, J. J. Cooperativity in amide hydrogen bonding chains: implications for protein-folding models. *J. Am. Chem. Soc.* **2001**, *123*, 4348−4349.
(27) Hollamby, M. J.; Aratsu, K.; Pauw, B. R.; Rogers, S. E.; Smith, A. J.; Yamauchi, M.; Lin, X.; Yagai, S. Simultaneous SAXS and SANS analysis for the detection of toroidal supramolecular polymers composed of noncovalent supermacrocycles in solution. *Angew. Chem.* **2016**, *128*, 10044−10047.
(28) Filot, I. A. W.; Palmans, A. R. A.; Hilbers, P. A. J.; van Santen, R. A.; Pidko, E. A.; de Greef, T. F. A. Understanding Cooperativity in Hydrogen-Bond-Induced Supramolecular Polymerization: A Density Functional Theory Study. *J. Phys. Chem. B* **2010**, *114*, 13667−13674.
(29) Nakano, Y.; Hirose, T.; Stals, P. J. M.; Meijer, E. W.; Palmans, A. R. A. Conformational analysis of supramolecular polymerization processes of disc-like molecules. *Chem. Sci.* **2012**, *3*, 148−155.
(30) Kulkarni, C.; Meijer, E. W.; Palmans, A. R. A. Cooperativity scale: a structure mechanism correlation in the self assembly of benzene-1,3,5-carbozamides. *Acc. Chem. Res.* **2017**, *50*, 1928−1936.
(31) Smulders, M. M. J.; Nieuwenhuizen, M. M. L.; de Greef, T. F. A.; van der Schoot, P.; Schenning, A. P. H. J.; Meijer, E. W. How to distinguish isodesmic from cooperative supramolecular polymerisation. *Chem. - Eur. J.* **2010**, *16*, 362−367.
(32) ten Eikelder, H. M. M.; Markvoort, A. J.; de Greef, T. F. A.; Hilbers, P. A. J. An equilibrium model for chiral amplification in supramolecular polymers. *J. Phys. Chem. B* **2012**, *116*, 5291−5301.
(33) Zhao, D.; Moore, J. S. Nucleation−elongation: a mechanism for cooperative supramolecular polymerization. *Org. Biomol. Chem.* **2003**, *1*, 3471−3491.
(34) Korevaar, P. A.; Schaefer, C.; de Greef, T. F. A.; Meijer, E. W. Controlling chemical self-assembly by solvent-dependent dynamics. *J. Am. Chem. Soc.* **2012**, *134*, 13482−13491.
(35) Hansen, M. R.; Graf, R.; Spiess, H. W. Interplay of structure and dynamics in functional macromolecular and supramolecular systems as revealed by magnetic resonance spectroscopy. *Chem. Rev.* **2016**, *116*, 1272−1308.
(36) Weingarth, M.; Baldus, M. Solid-state NMR-based approaches for supramolecular structure elucidation. *Acc. Chem. Res.* **2013**, *46*, 2037−2046.
(37) Hansen, M. R.; Graf, R.; Spiess, H. W. Solid-state NMR in macromolecular systems: insights on how molecular entities move. *Acc. Chem. Res.* **2013**, *46*, 1996−2007.
(38) Tasios, N.; Grigoriadis, C.; Hansen, M. R.; Wonneberger, H.; Li, C.; Spiess, H. W.; Müllen, K.; Floudas, G. Self-assembly, dynamics, and phase transformation kinetics of donor−acceptor substituted perylene derivatives. *J. Am. Chem. Soc.* **2010**, *132*, 7478−7487.
(39) Hansen, M. R.; Graf, R.; Sekharan, S.; Sebastiani, D. Columnar packing motifs of functionalized perylene derivatives: local molecular order despite long-range disorder. *J. Am. Chem. Soc.* **2009**, *131*, 5251−5256.
(40) Seifrid, M.; Reddy, G. N. M.; Chmelka, B. F.; Bazan, G. C. Insight into the structures and dynamics of organic semiconductors through solid-state NMR spectroscopy. *Nat. Rev. Mater.* **2020**, *5*, 910−930.
(41) Reddy, G. N. M.; Huqi, A.; Iuga, D.; Sakurai, S.; Marsh, A.; Davis, J. T.; Masiero, S.; Brown, S. P. Co-existence of distinct supramolecular assemblies in solution and in the solid State. *Chem. - Eur. J.* **2017**, *23*, 2315−2322.
(42) Reddy, G. N. M.; Marsh, A.; Davis, J. T.; Masiero, S.; Brown, S. P. Interplay of noncovalent interactions in ribbon-like guanosine self-assembly: an NMR crystallography study. *Cryst. Growth Des.* **2015**, *15*, 5945−5954.
(43) Seifrid, M. T.; Reddy, G. N. M.; Zhou, C.; Chmelka, B. F.; Bazan, G. C. Direct observation of the relationship between molecular topology and bulk morphology for a π-conjugated material. *J. Am. Chem. Soc.* **2019**, *141*, 5078−5082.
(44) Hansen, M. R.; Schnitzler, T.; Pisula, W.; Graf, R.; Müllen, K.; Spiess, H. W. Cooperative molecular motion within a self-assembled

liquid-crystalline molecular wire: the case of a TEG-substituted perylenediimide disc. *Angew. Chem., Int. Ed.* **2009**, *48*, 4621−4624.
(45) Webber, A. L.; Masiero, S.; Pieraccini, S.; Burley, J. C.; Tatton, A. S.; Iuga, D.; Pham, T. N.; Spada, G. P.; Brown, S. P. Identifying guanosine self assembly at natural isotopic abundance by high-resolution ^{1}H and ^{13}C solid-state NMR spectroscopy. *J. Am. Chem. Soc.* **2011**, *133*, 19777−19795.
(46) Carter-Fenk, K.; Herbert, J. M. Electrostatics does not dictate the slip-stacked arrangement of aromatic $\pi-\pi$ interactions. *Chem. Sci.* **2020**, *11*, 6758−6765.
(47) Wurthner, F.; Saha-Moller, C. R.; Fimmel, B.; Ogi, S.; Leowanawat, P.; Schmidt, D. Perylene bisimide dye assemblies as archetype functional supramolecular materials. *Chem. Rev.* **2016**, *116*, 962−1052.
(48) Smulders, M. M. J.; Schenning, A. P. H. J.; Meijer, E. W. Insight into the mechanisms of cooperative self-assembly: the sergeants-and-soldiers principle of chiral and achiral C_3-symmetric discotic triamides. *J. Am. Chem. Soc.* **2008**, *130*, 606−611.
(49) Shao, C.; Grüne, M.; Stolte, M.; Würthner, F. Perylene bisimide dimer aggregates: fundamental insights into self-assembly by NMR and UV/vis Spectroscopy. *Chem. - Eur. J.* **2012**, *18*, 13665−13677.
(50) Sao, S.; Naskar, S.; Mukhopadhyay, N.; Das, M.; Chaudhuri, D. Assisted π-stacking: a strong synergy between weak interactions. *Chem. Commun.* **2018**, *54*, 12186−12189.
(51) Samanta, S.; Mukhopadhyay, N.; Chaudhuri, D. Rapid and efficient electrochemical actuation in a flexible perylene bisimide dimer. *Chem. Mater.* **2019**, *31*, 899−903.
(52) Harris, R. K.; Jackson, P.; Merwin, L. H.; Say, B. J.; Hägele, G. Perspectives in high-resolution solid-state nuclear magnetic resonance, with emphasis on combined rotation and multiple-pulse spectroscopy. *J. Chem. Soc., Faraday Trans. 1* **1988**, *84*, 3649−3672.
(53) Bradley, J. P.; Tripon, C.; Filip, C.; Brown, S. P. Determining relative proton−proton proximities from the build-up of two-dimensional correlation peaks in ^{1}H double-quantum MAS NMR: insight from multi-spin density-matrix simulations. *Phys. Chem. Chem. Phys.* **2009**, *11*, 6941−6952.
(54) Goldstein, R. F.; Stryer, L. Cooperative polymerization reactions: analytical approximations, numerical examples, and experimental strategy. *Biophys. J.* **1986**, *50*, 583−599.
(55) Manjunatha Reddy, G. N.; Peters, G. M.; Tatman, B. P.; Rajan, T. S.; Kock, S. M.; Zhang, J.; Frenguelli, B. G.; Davis, J. T.; Marsh, A.; Brown, S. P. Magic-angle spinning NMR spectroscopy provides insight into the impact of small molecule uptake by G-quartet hydrogels. *Mater. Adv.* **2020**, *1*, 2236−2247.
(56) Disruption of hydrogen-bonding and a subsequent disassembly can be carried out using either ^{t}BuOH or ethanol. In absorption spectroscopy experiments, we used the former because of its higher boiling point that allowed us to accurately and reproducibly maintain a low volume fraction (f). In ^{1}H-NMR titration experiments, ethanol-*d* was used.
(57) Both ethanol and $CHCl_3$ eventually disassemble the aggregate completely. The NMR titration experiment probes the early stages of aggregate disassembly, where only one interaction is preferentially disrupted.

https://doi.org/10.1021/acscentsci.1c00604
ACS Cent. Sci. 2021, 7, 1391−1399